Supplementary Information

Development of High Surface Area Cu Electrocatalyst for Effective Nitrous Oxide Reduction Reaction

Siraphat Nilvichean,[1] Kornkamon Meesombad,[2] Teera Butburee,[2] Pongkarn Chakthranont,[*2] and Rungthiwa Methaapanon[*1]

[1] Centre of Excellence in Particle and Material Processing Technology, Department of Chemical Engineering, Chulalongkorn University, Bangkok, Thailand 10330

[2] National Nanotechnology Center (NANOTEC), National Science and Technology Development Agency (NSTDA), Pathum Thani, Thailand 12120

Corresponding authors: pongkarn.cha@nanotec.or.th, rungthiwa.m@chula.ac.th

Table S1. Activities of the reported N_2ORR catalysts and their testing conditions

Catalyst	Cell type	Electrolyte	j_{max} (mA cm^{-2}) (E, V vs RHE)	FE* of N_2 at j_{max}	E_{onset} (V vs RHE)	Tafel slope (mV dec^{-1})	Ref.
High surface area Cu	H-cell	0.1 M KOH	10.0 (-0.2 V)	83.3%	0.27	124	This work
Cu metal	H-cell	0.3 M K$_2$SO$_4$	8 (-0.31 V)	78%	N/A	N/A	[1]
Polycrystal Cu	RDE**	0.3 M K$_2$SO$_4$	43.75 (-0.8 V)	N/A	-0.56	N/A	[2]
In/Cu foam	H-cell	0.5 M NaOH	25 (-0.75 V)	~100%	<0	N/A	[3]
ZnO	H-cell	0.3 M K$_2$SO$_4$	6.8 (-0.82 V)	91%	N/A	N/A	[1]
In$_2$O$_3$	H-cell	0.3 M K$_2$SO$_4$	8.5 (-0.47 V)	82%	N/A	N/A	[1]
SnO$_2$	H-cell	0.3 M K$_2$SO$_4$	6.6 (-0.57 V)	73%	N/A	N/A	[1]
Polycrystal Pd	RDE	0.1 M NaOH	20 (0 V)	N/A	0.64	84	[4]
Pd$_{60}$Cu$_{40}$	H-cell	0.3 M K$_2$SO$_4$ and 0.2 M KOH	6.0 (0.04 V)	N/A	0.73	96	[5]
Au@Pd	RDE	0.2 M K$_2$SO$_4$ and 0.3 M KOH	N/A	N/A	0.84	105	[6]
Polycrystal Pt	RDE	0.1 M NaOH	7.4 (0.2 V)	N/A	0.5	111	[4]
Pt on gas diffusion electrode	Flow cell	1 M KOH	130 (0 V)	100%	0.44	N/A	[7]
Ir (100)	N/A	0.1 M HClO$_4$	Inactive	N/A	N/A	N/A	[8]
Ir (111)	N/A	0.1 M HClO$_4$	~0.85 (~0.1 V)	N/A	~0.3	N/A	[8]
Ir (110)	N/A	0.1 M HClO$_4$	~0.75 (~0.1 V)	N/A	~0.3	N/A	[8]

*Faradaic efficiency (FE) of N_2 can be calculated only if the gas product is quantified. Most of the N_2ORR studies reported in the literature have not performed any product detection for N_2 or H_2.

** Rotating disk electrode (RDE) employs rotation motion to improve the mass transport of N_2O to the electrode, which leads to a higher j_{max} than H-cell system; however, product detection is not feasible in this setup as the electrochemical cell is not gas-tight.
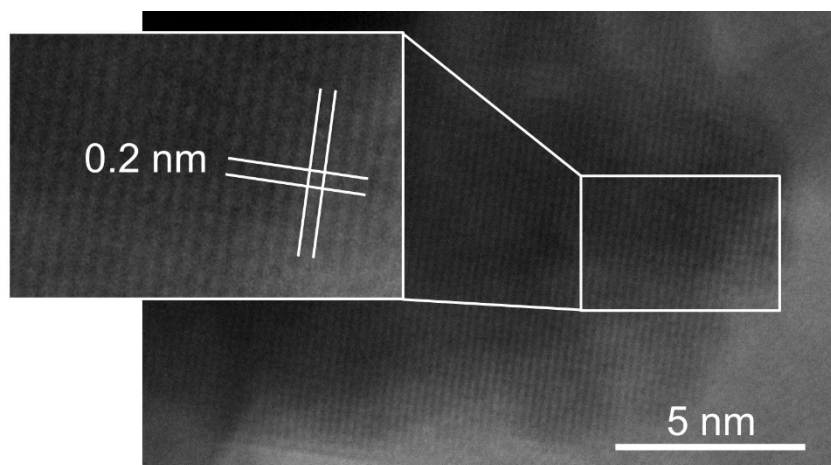
Figure S1. High resolution transmission electron microscopy (HRTEM) image of Cu_2O electrodeposited at 40 °C for 30 minutes exhibits 0.2 nm lattice fringes associated with the (200) planes of Cu_2O.

a

RMS roughness (S_q):	12.7846	nm
Mean roughness (S_a):	10.6734	nm
Projected area:	622.236	µm²
Surface area:	622.592	µm²
Surface ratio:	1.0006	

b

|	Cu-20 min	Cu-30 min	Cu-40 min
RMS roughness (S_q) (nm)	90.9759	212.49	355.321
Mean roughness (S_a) (nm)	72.5034	165.94	280.625
Projected area (µm²)	627.443	627.443	627.443
Surface area (µm²)	699.47	699.065	813.906
Surface ratio	1.1148	1.1141	1.2972
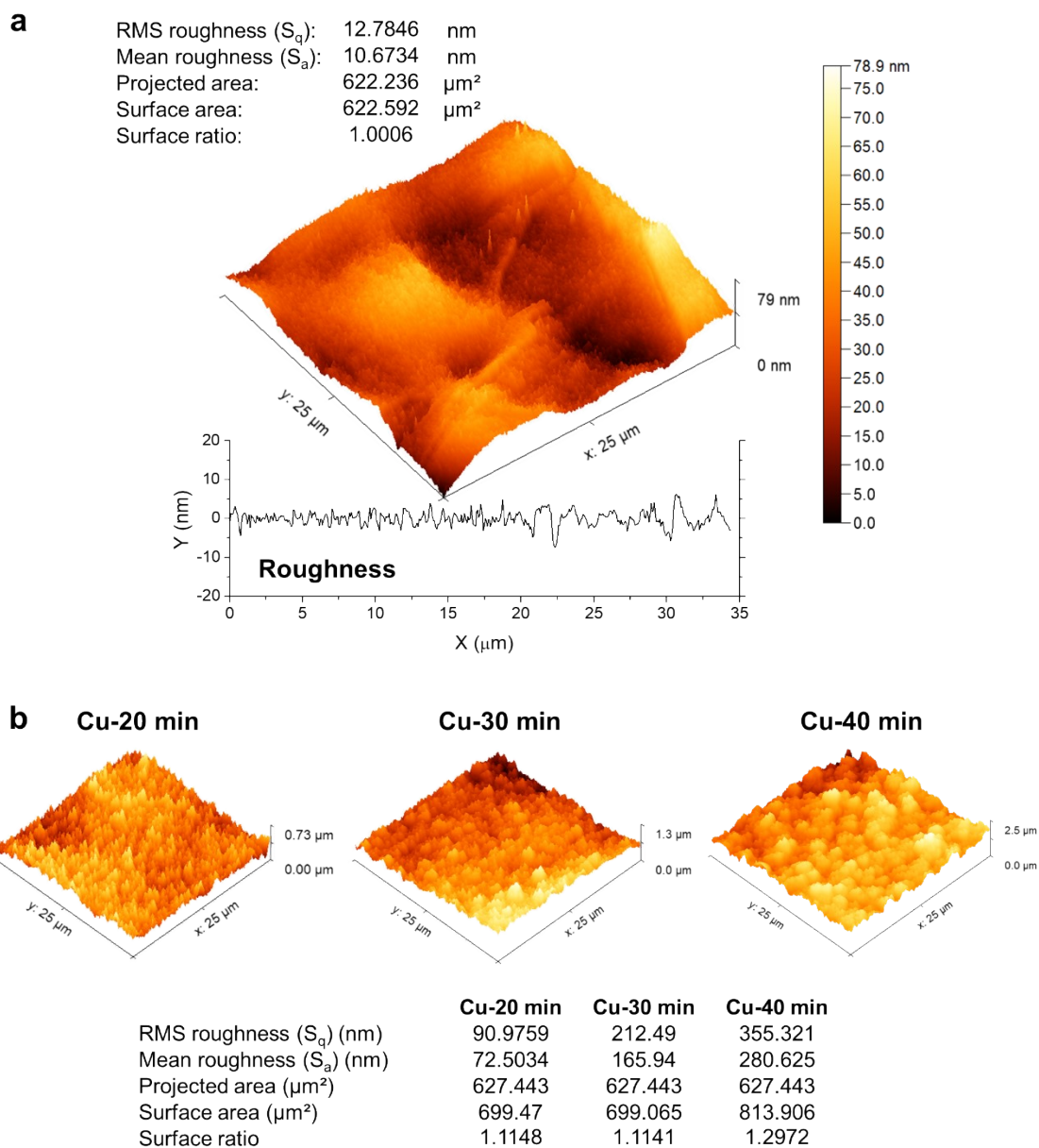
Figure S2. (a) AFM measurements of the roughness, surface area, and surface ratio (real surface area/projected surface area) of electropolished Cu foil confirm that the Cu-Epolish sample was significantly flat (surface ratio = 1) and can be used to calculate the true electrochemically active surface area (ECSA) of the high surface area electrodes. (b) Surface morphologies of Cu_2O electrodeposited at 40 °C for 20, 30, and 40 min as characterized by AFM. Due to the highly porous structure of electrodeposited Cu_2O, the surface area ratio from AFM would underestimate the actual surface areas of these high surface area electrodes.
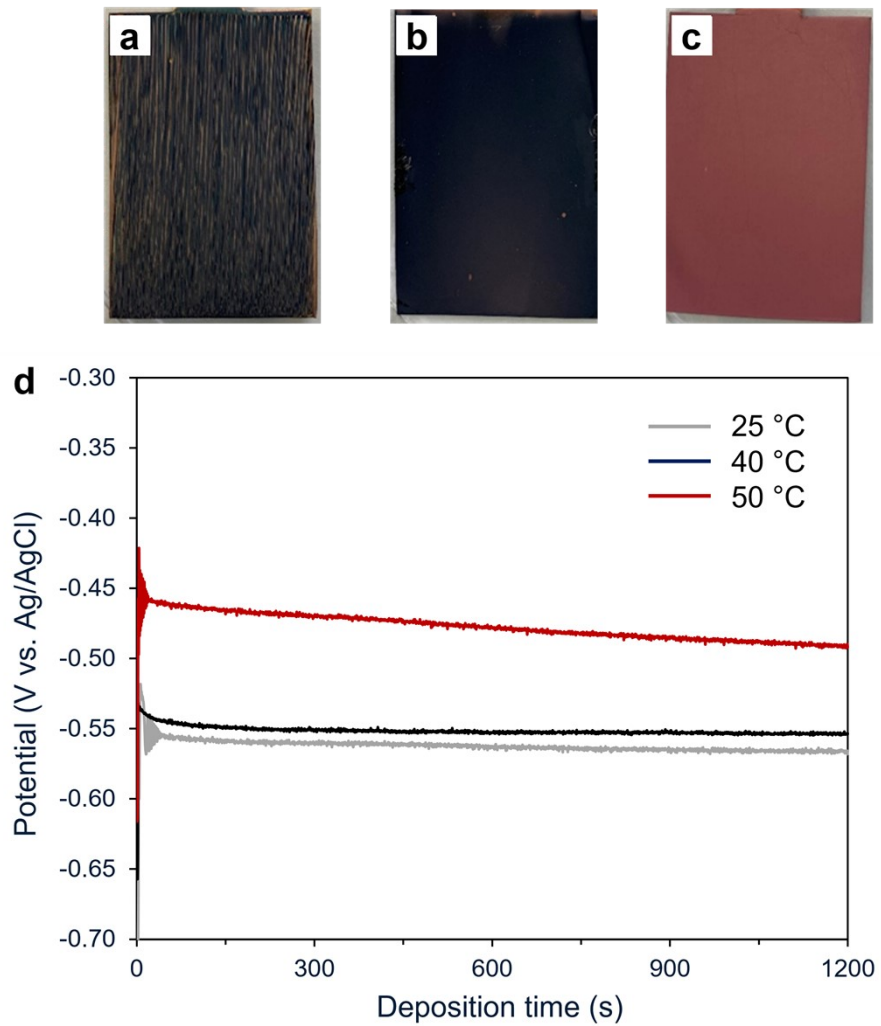
Figure S3. Photos of the Cu_2O electrodes deposited at (a) 25 °C, (b) 40 °C, and (c) 50°C. (d) Deposition potentials of the Cu_2O electrodes conducted at a fixed current density of -1.7 mA cm^{-2} for 20 min at varying temperatures.

a

b
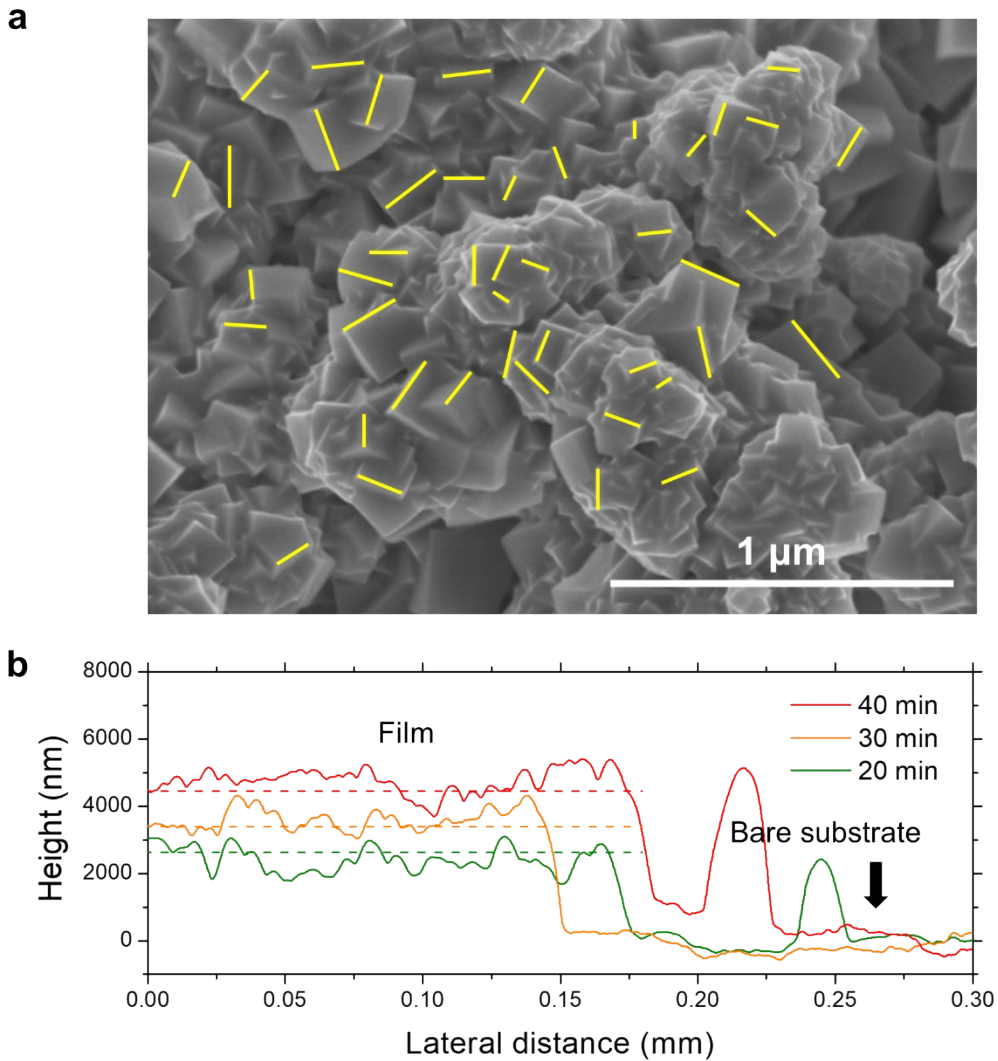
Figure S4. (a) Example of particle size measurement from edge-to-edge lengths of cubic particles. (b) Thickness profiles of Cu_2O films deposited at 40 °C for 20, 30, and 40 min measured by a stylus profiler.
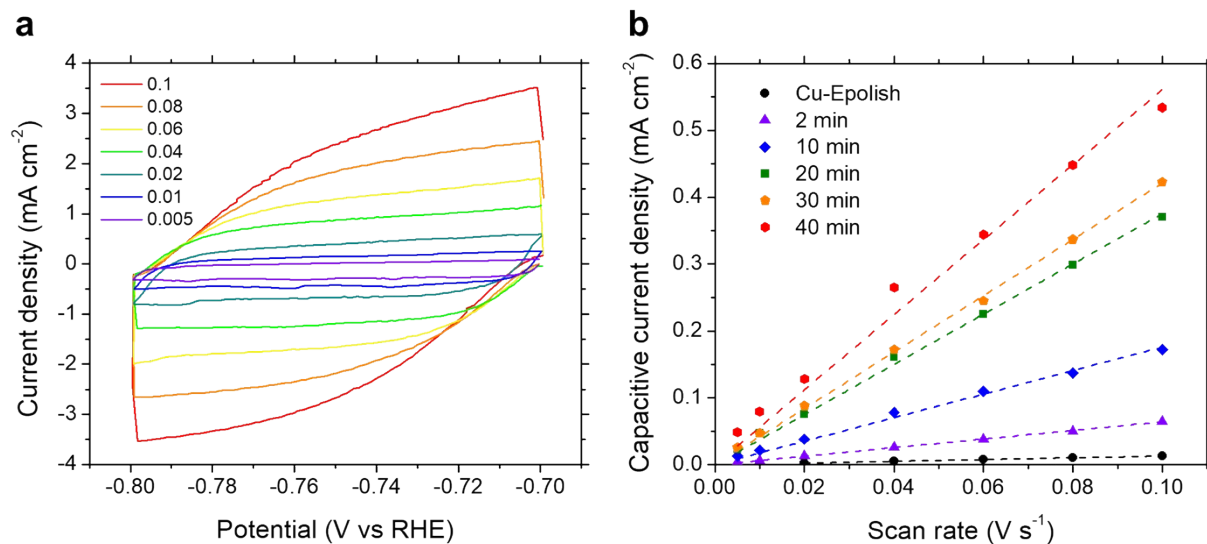
Figure S5. (a) Cyclic voltammograms in the non-Faradaic region of the reduced Cu-30 min electrode measured at varying scan rates (in V/s). (b) Capacitive current densities (
$$j_{dl} = \frac{j_{anodic} - J_{cathodic}}{2}$$
) of all Cu electrodes measured at -0.75 V vs Ag/AgCl at varying scan rates; the slopes correspond to the double-layer capacitance (C_{dl}). The C_{dl} of Cu-Epolish of 0.14 mF cm^{-2} was used as a basis for the roughness factor calculation.
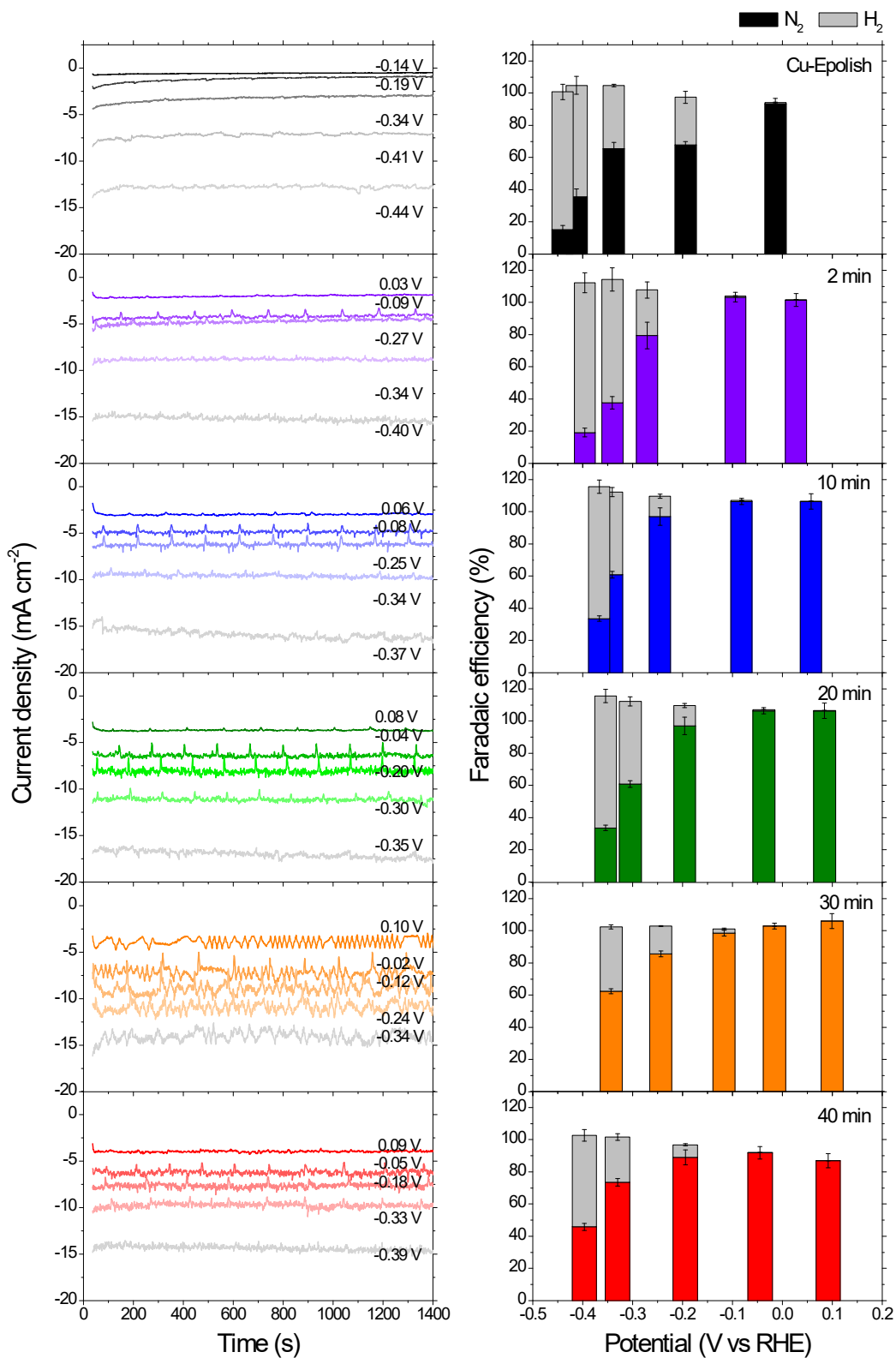
Figure S6. Chronoamperometry current densities and Faradaic efficiencies at varying potentials of all catalysts. The electrolysis experiments were conducted in 0.1 M KOH under a 20 mL min^{-1} N$_2$O gas flow rate.

Table S2. Randles circuit components extracted from the Nyquist spectra of Cu-Epolish and Cu-30 min measured at varying potentials

| E (V vs RHE)	Cu-Epolish				Cu-30 min			
	R_{ct} (Ω)	Q_{dl}	$\propto$	C_{dl}* (mF cm^{-2})	R_{ct} (Ω)	Q_{dl}	$\propto$	C_{dl}* (mF cm^{-2})
-0.18	16.95	4.38E-04	0.92	0.048	17.34	2.64E-02	0.90	4.04
-0.29	8.18	3.69E-04	0.92	0.037	7.85	2.48E-02	0.89	3.37
-0.39	5.01	1.02E-03	0.87	0.075	4.60	1.35E-02	0.86	1.43

The capacitance per unit area can be calculated from constant phase element (Q), constant phase ($\propto$), and electrode geometric area (A = 6 cm^2) as follow:

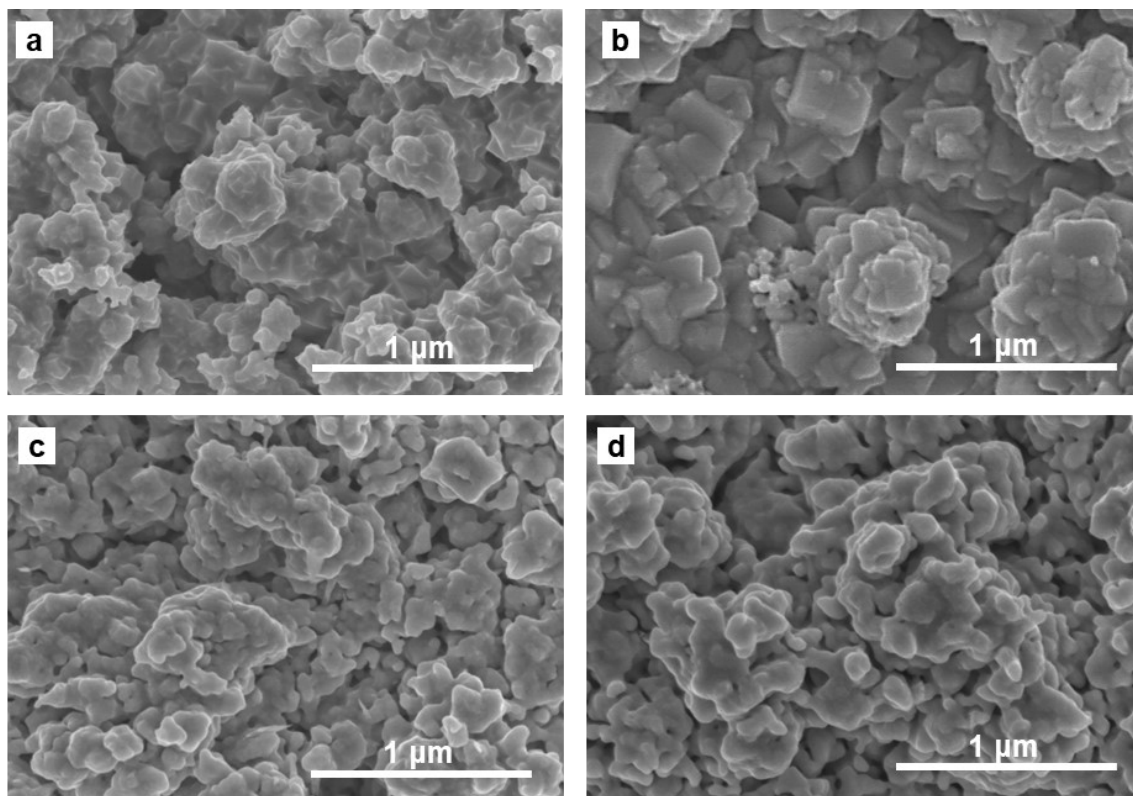$$C[mF\,cm^{-2}] = \frac{(QR)^{\frac{1}{\propto}}}{1000 * R * A[cm^2]}$$

The average roughness factor of Cu-30 min calculated from EIS ($C_{dl\,Cu\text{-}30\,min}/C_{dl\,Cu\text{-}Epolish}$) is 55.37.
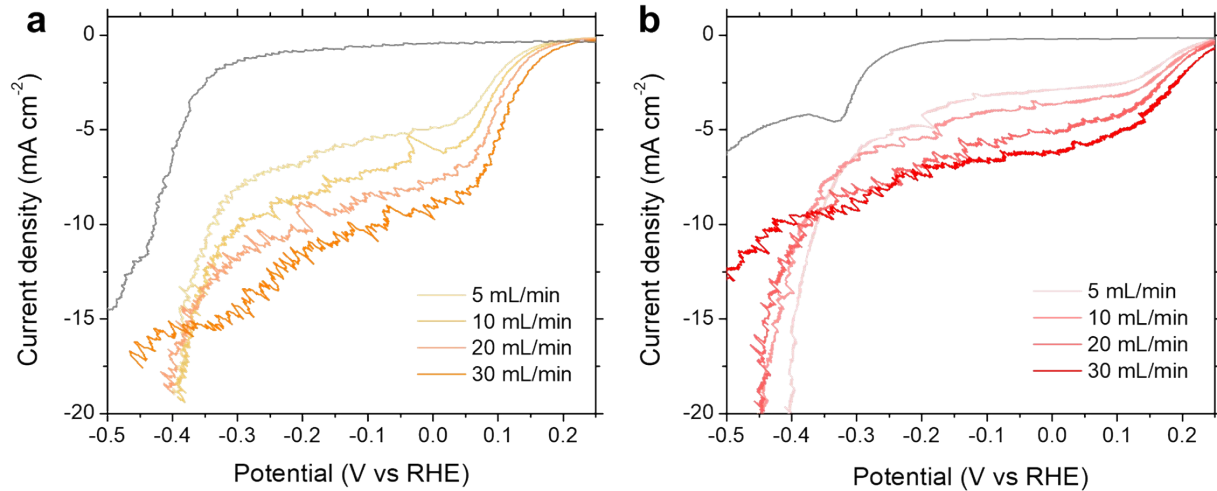
Figure S7. Effects of N$_2$O flow rate on the current-voltage curves of (a) Cu-30 min and (b) Cu-40 min.
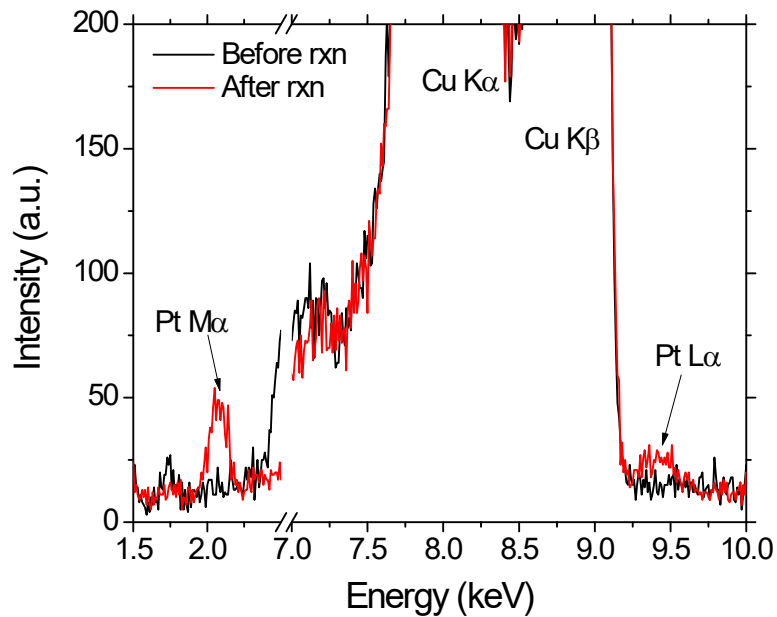
Figure S8. XRF spectrum of Cu-30 min catalyst before and after 7 h testing in N_2ORR condition at 0.12 V vs RHE.

Figure S9. SEM images of Cu-30 min sample: (a) as-deposited Cu_2O, (b) after electrochemical reduction by CV, (c) after a typical N_2ORR experiment, and (d) after 7 h stability testing.

References

1. A. Kudo and A. Mine, *Applied Surface Science*, 1997, **121-122**, 538-542.
2. O. J. S. Kwon, S. Baek, H. Kim, I. Choi, O. J. S. Kwon and J. J. Kim, *Electroanalysis*, 2019, **31**, 739-745.
3. K. H. Kim, T. Lim, M. J. Kim, S. Choe, S. Baek and J. J. Kim, *Electrochemistry Communications*, 2016, **62**, 13-16.
4. A. Aziznia, A. Bonakdarpour, E. L. Gyenge and C. W. Oloman, *Electrochimica Acta*, 2011, **56**, 5238-5244.
5. S. Baek, K. Kim, O. S. Kwon, H. Kim, J. W. Han, O. J. Kwon and J. J. Kim, *Journal of Applied Electrochemistry*, 2020, **50**, 395-405.
6. K. Kim, J. Byun, H. Kim, K.-S. Lee, H. S. Lee, J. Kim, T. Hyeon, J. J. Kim and J. W. Han, *ACS Catalysis*, 2021, **11**, 15089-15097.
7. N. Furuya and H. Yoshiba, *Journal of Electroanalytical Chemistry*, 1991, **303**, 271-275.
8. R. Gómez and M. J. Weaver, *Langmuir*, 2002, **18**, 4426-4432.